Prediction of Rotational Stabilisation of Resistive Wall Modes in ITER

T C Hender 1), H Reimerdes 2), M S Chu 3), A M Garofalo 2), M P Gryaznevich 1), D F Howell 1), R J La Haye 3), Y Q Liu 4), M Okabayashi 5), S D Pinches 1), E J Strait 3), the DIII-D Team and JET EFDA Contributors[§]

1) Euratom/UKAEA Fusion Association, Culham Science Centre, Abingdon, OX14 3DB, UK
2) Columbia University, New York, New York 10027, USA
3) General Atomics, P.O. Box 85608, San Diego, California 92186-5608, USA
4) Association Euratom-VR, Chalmers University of Technology, Göteborg, Sweden
5) Princeton Plasma Physics Laboratory, Princeton, New Jersey 08543–0451, USA
[§]See the Appendix of M. L. Watkins et al., Fusion Energy 2006 (Proc. 21st Int. Conf. Chengdu, 2006) IAEA, (2006)

E-mail address of main author:- tim.hender@ukaea.org.uk

Abstract. In advanced tokamak operation the ultimate performance limit is set by resistive wall modes (RWMs). A damping term arising from relative rotation between the plasma and mode determines the stability of the RWM and cross machine experiments, between DIII-D and JET, aimed at determining this damping are reported. Comparisons of the amplification factors of applied resonant fields show good agreement between JET, DIII-D and calculations with the MARS-F code using a kinetic damping model. A second comparison using n=1 magnetic braking to determine the critical velocity at which RWMs are destabilised is also presented. The interpretation of this result is discussed in view of the fact that the applied fields may be playing a role in driving the observed mode. The results can however be interpreted as providing a threshold for applied error fields to destabilise RWMs and illustrate the importance of error field correction at high-β in ITER.

1. Introduction

The ultimate performance limit is set by resistive wall modes (RWMs) [1] in advanced tokamak operating scenarios, such as those foreseen for ITER and compatible with the steady-state operation of a power plant. The RWM is a kink mode whose stability is related to damping arising from relative rotation between the fast rotating plasma and the slowly rotating wall mode. Plasma rotation, and the ensuing RWM damping, is a passive stabilising mechanism making it an attractive route for RWM control. It is thus important to understand how plasma rotational stabilisation of the RWM will scale to ITER and future power plants. The nature of this stabilisation is still under study and several models have been studied, e.g. an empirical sound wave damping model [1] and a 'kinetic' model [2] which has no free fitting parameters. A range of other damping models and mechanisms have also been proposed, e.g. [3,4,5]. Cross machine scaling studies [6] represent a good way of testing the various theories on RWM damping – in this paper such cross machine RWM studies between JET and DIII-D are presented. An excellent way of probing RWM stability has been to examine the plasma response to externally applied resonant fields [7,8]. As the β-limit without the stabilising influence of surrounding walls (β_N(no-wall)) is exceeded, strong Resonant Field Amplification (RFA), which depends on the plasma damping, occurs. Cross machine studies of RFA are discussed below. A second way of probing RWM stability is to

compare the critical rotation velocity below which an n=1 RWM is destabilised, and studies comparing JET and DIII-D results on this issue are also discussed below; these studies used magnetic braking to slow the plasma and the implications of this will be examined.

2. Experimental setup

The JET/DIII-D RWM studies are based on plasmas with closely matched boundary shape, and reasonably matched safety factor (q) and pressure profiles. In terms of internal inductance, ℓ_i, defined as $\left\langle B_p^2 \right\rangle / \left\langle B_p \right\rangle^2$, it is found that the no-wall β-limit is $\beta_N \sim 2.8\ell_i$ in both JET and DIII-D, though higher edge current in DIII-D contributes to a lower underlying ℓ_i. The main parameters typical of these experiments are summarised in Table 1.

Table 1 Comparison of typical parameters in DIII-D and JET for joint RWM experiments. The wall time is the decay time for an m=1 field.

	DIII-D	JET
Major Radius (m)	1.69	2.96
Toroidal Field B_T(T)	1.8-2.1	0.8-1.4
Elongation	1.7	1.7
Wall Time(ms)	7.0	6.3
Internal inductance (ℓ_i)	0.7	0.95
Ideal MHD no wall β_N limit	2.0 ($2.8\ell_i$)	2.7 ($2.8\ell_i$)
Ideal MHD ideal wall β_N limit	3.0	3.6
Central electron temperature $T_{e,0}$(keV)	3.1	4.0
Central electron density $n_{e,0}$(10^{19}/m^3)	6.3	2.7
Alfvén time (μs)	0.5	0.85
Sound time(μs)	2.8	4.8

In the RWM experiments described here, non-axisymmetric (dominantly n=1) fields are applied using the C-coils in DIII-D and the error field corrections coils (EFCCs) in JET (see Fig 1). The resulting RWM behaviour is measured using radial field detectors mounted just outside the vessel (Fig 1).

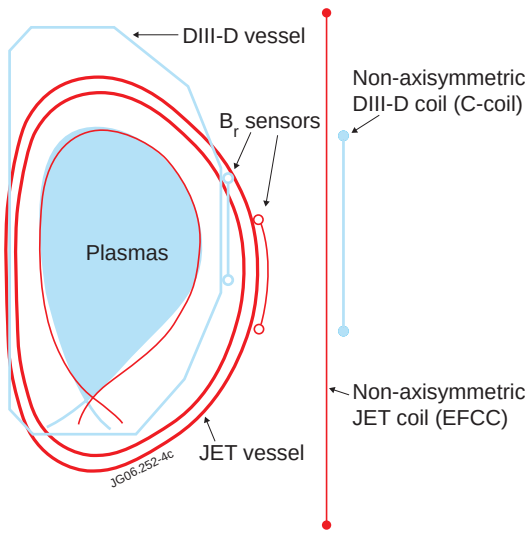

Fig 1 Comparison of JET (red lines) and DIII-D (blue lines) plasmas, vessel geometry and non-axisymmetric coils used in cross machine RWM experiments

3. Resonant Field Amplification

In the RFA experiments the plasma response of rotationally stabilised plasmas as a function of β, to applied non-axisymmetric fields, has been compared between JET and DIII-D (Fig 2). It can be seen from Fig 1 that there are significant geometric differences between exciting and measuring coils, in JET and DIII-D. To correct for this the decrease of the externally applied field from the sensor to the plasma and the decrease of the plasma response from the plasma to the sensor need to be taken into account. Defining the RFA as the ratio of the amplitude of the plasma response (B_r^{Plas}) to the amplitude of the applied radial field (B_r^{Ext}), in a cylindrical approximation the ratio of the RFA at the plasma boundary ($r=a$) and the RFA measured with a sensor ($r= r_{sen}$) is,

$$\frac{B_r^{Plas}(r=a)/B_r^{Ext}(r=a)}{B_r^{Plas}(r=r_{sen})/B_r^{Ext}(r=r_{sen})} = \left(\frac{r_{sen}}{a}\right)^{2m}$$

where m is the poloidal mode number. Assuming an effective poloidal mode number of m=2, the RFA at the DIII-D plasma boundary is 3.5 times larger than at the DIII-D sensors, whereas the RFA at the JET boundary is 8.25 times larger than at the JET sensors. The data in Fig 2 have this correction applied so that the RFA at the plasma boundary are being compared. Also in Fig 2 the measured radial field ($B_r(\phi=90^o)$) at the node of applied field is used (so that in the absence of a plasma the measured B_r=0), meaning the RFA is defined as, RFA= $\left| B_r(\phi=90^o) \right| / \left| B_r(\phi=0^o) \right|$.

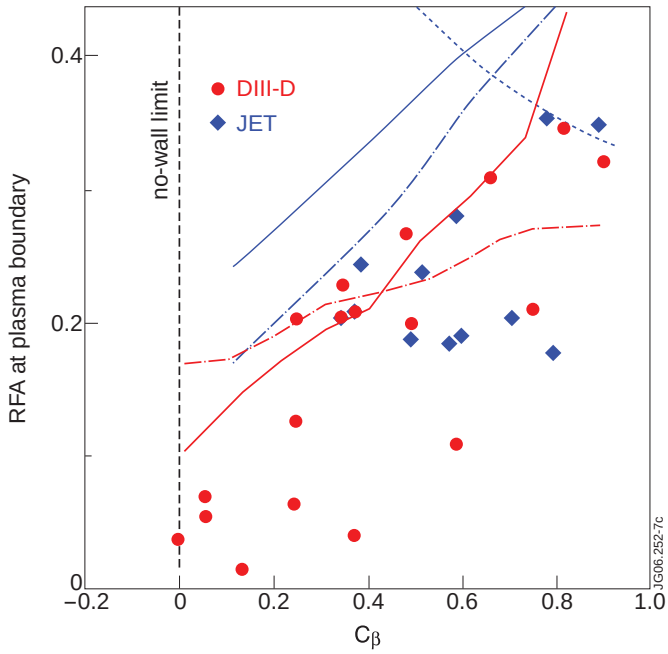

Fig 2 RFA versus C_β =(β_N- β_N(no wall)) /(β_N(with wall) – β_N(no wall)). Geometric differences between the JET and DIII-D coil system are accounted for, as explained in the text. Here the broken dash-dot lines are calculations using the kinetic damping model in the MARS-F MHD stability code [9]. The solid lines are the sound wave model with strong damping ($\kappa_{||}$=1.5) and the dotted line is weak damping ($\kappa_{||}$=0.1). The red lines are based on a DIII-D equilibrium and the blue lines on a JET equilibrium (for clarity the weak kinetic damping model is not shown for DIII-D - the agreement is equally as bad as for the JET case)

From Fig 2, it can be seen that there is reasonable agreement on the RFA between JET and DIII-D, once the geometrical differences are taken into account; though the approximate nature of the geometric correction applied and differences in the applied spectrum of fields in

JET and DIII-D should be kept in mind. The scatter of the data in Fig 2 is in part be due to the accuracy with which the stability of each discharge is determined (C_β values). The absolute rotation velocities in DIII-D are higher, but when scaled to the Alfvén time (τ_A(JET)/ τ_A(DIII-D)~1.6) agree reasonably with those in JET at q=2. Thus given the similarity of the equilibria in JET and DIII-D, the results are consistent with damping which depends on the plasma velocity near q=2 normalised to τ_A. Also shown in Fig 2 is a comparison with MARS-F stability code [9] predictions using the kinetic damping and sound wave damping models. The kinetic damping model [2] which is based on drift-kinetic theory predicts the damping arising from forces acting on displacements perpendicular to the magnetic field; it is important to note that this kinetic model has no free fitting parameters. A more ad-hoc sound wave damping model is also implemented in MARS-F and shown in Fig 2. In this model the force that damps the *(m,n)* Fourier component of the perturbed toroidal motion of the plasma is represented as a parallel viscosity term, $F_{damp} = -\kappa_{||} | k_{||} v_{th,i} | \rho v_{||}$. Here, $k_{||} = (m/q - n)/R$ is the parallel wave number, $v_{th,i}$ is the ion thermal velocity, ρ is the mass density, $v_{||}$ the perturbed parallel velocity of the plasma and $\kappa_{||}$ is a constant whose value may be empirically determined by fitting to experimental results. In addition to these explicit damping models MARS-F also implicitly includes continuum Alfvén damping. It can be seen that the kinetic model and strong sound wave damping ($\kappa_{||}$=1.5) models are in reasonable agreement with the RFA data in Fig 2. A possible way of discriminating between the kinetic damping and strong sound wave damping model is discussed in Section 5.

4. Critical Velocity

The critical velocity below which the RWM is destabilised (Ω_{crit}) has also been compared between JET and DIII-D. In these experiments the dominantly n=1 applied non-axisymmetric field amplitude is gradually increased, which brakes the plasma and allows an RWM to be destabilised if $\beta > \beta_{no\text{-}wall}$ [10]. It is found that $\Omega_{crit}(q=2)$ normalised by τ_A is approximately the same in JET and DIII-D (filled symbols in Fig 3). At the magnetic axis $\tau_A \Omega_{crit}$ differs significantly between JET and DIII-D (Fig 3) – thus suggesting the damping occurs in the vicinity of q=2 (where the $\tau_A \Omega_{crit}$ values are in approximate agreement). Also shown in Fig 3 are the predictions of the $\tau_A \Omega_{crit}$ values from the MARS-F code using the kinetic damping model for the range of C_β encompassed by the experimental data. As with the RFA comparison it can be seen that the kinetic model gives reasonable agreement with the data showing $\tau_A \Omega_{crit}$~0.5% at q=2.

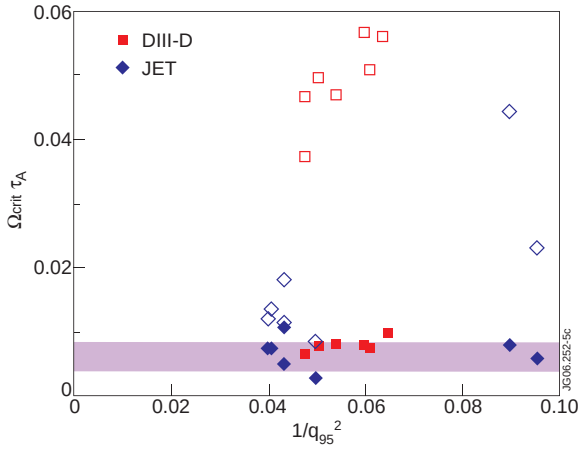

Fig 3 $\Omega_{crit}\ \tau_A$ as function of $(1/q_{95})^2$, filled symbols are at q=2 and open at the axis. The shaded band is the MARS-F kinetic model prediction at q=2 for the range of experimental C_β.

In the above, the critical velocity is determined by braking the plasma using externally applied fields. At low-β, application of externally applied fields (e.g. with an m=2, n=1 component) is known to drive locked modes in otherwise stable plasmas [11,12] and the question arises whether the modes observed here are at least in part driven by the applied error field? This issue is further highlighted by recent DIII-D experiments using balanced beams which show values for the RWM critical velocity substantially below those in the magnetic braking experiments [13]. Comparison of the growth of the mode destabilised by the application of external fields at low-β (Ohmic pulses) and in the 'RWM' magnetic braking experiments does show growth rates at least a factor of 2 lower in the low-β pulses, and that the growth times of the 'RWM' pulses can approach 20ms (i.e. a few wall times), though this still somewhat slower than in DIII-D [6] (which has a similar wall time). Further, comparison of the poloidal structure of the mode that is destabilised at high-β (above the no-wall β-limit) does show moderately good agreement with the predicted RWM mode structure from MARS-F (Fig 4).

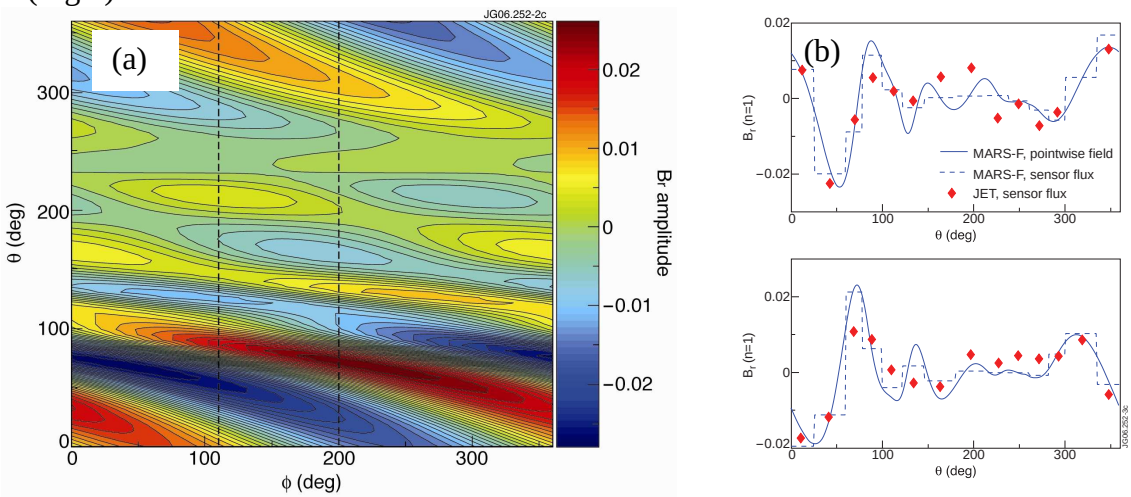

Fig 4 (a) Mode structure of the normal field at the JET vacuum vessel computed with the MARS-F code for an equilibrium similar to JET pulse 62646. Here θ is the poloidal angle starting at 0^o on the outboard mid-plane and increasing anti-clockwise, and ϕ is the toroidal angle (b) Comparison of measured odd-n radial field (red diamonds) shortly after magnetic braking destabilises a mode with the calculated variation from MARS-F taken at 2 toroidal angles separated by 90^o (as indicated by the broken lines in (a)). The broken lines in (b) are the MARS-F results taking account of the finite toroidal and poloidal extent of the sensor coils.

Thus it appears likely that the mode that is ultimately destabilised by the magnetic braking is an RWM, but this does not prove that the critical velocity measured using this technique is representative of the critical velocity for RWM destabilisation in the absence of applied error fields. An alternate interpretation of the data is that it represents the threshold for applied error fields to cause sufficient magnetic braking that an RWM is ultimately destabilised. Figure 5 shows the applied radial magnetic field at q=2 ($B_{2,1}$) that causes RWM onset in JET and DIII-D, as a function of C_β. It can be seen that the threshold error field decreases sharply with C_β and previous studies have shown below the no-wall limit (C_β <0) that the threshold increases sharply [10]. This data is important in terms of establishing the requirement for error field correction at high-β, and in fact indicates approximately the same correction requirements as at low-β, where an error field threshold of $B_{2,1}/B_T$~10^{-4} is found [14].

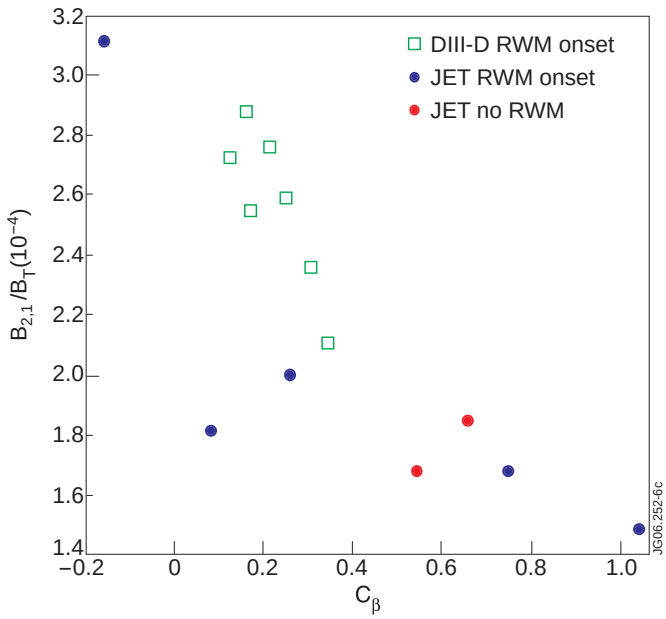

Fig 5 Threshold in applied error field ($B_{2,1}$) normalised to toroidal field to induce RWM onset in JET and DIII-D. Also shown for JET are 2 pulses where partial but not total magnetic braking occurs (so an RWM is not formed) – these are thought to be just below the marginal threshold.

5. Conclusions and Discussion

The n=1 RFA experiments provide a test of RWM damping models – comparisons indicate the kinetic damping model or strong sound wave damping are in reasonable agreement with the data. Experiments are planned on JET using n=2 applied field, where calculations with the MARS-F code indicate a better discrimination of the damping models should be possible, as shown in Fig 6. From this figure it can be seen that for n=1 the kinetic damping and strong sound wave damping models are quantitatively similar (as found before [10]), whereas for n=2 the weak sound wave damping model is quantitatively close to the predictions of the kinetic damping model. Thus study of the RFA for both n=1 and n=2 allows determination of which of the 3 models fits the data most satisfactorily.

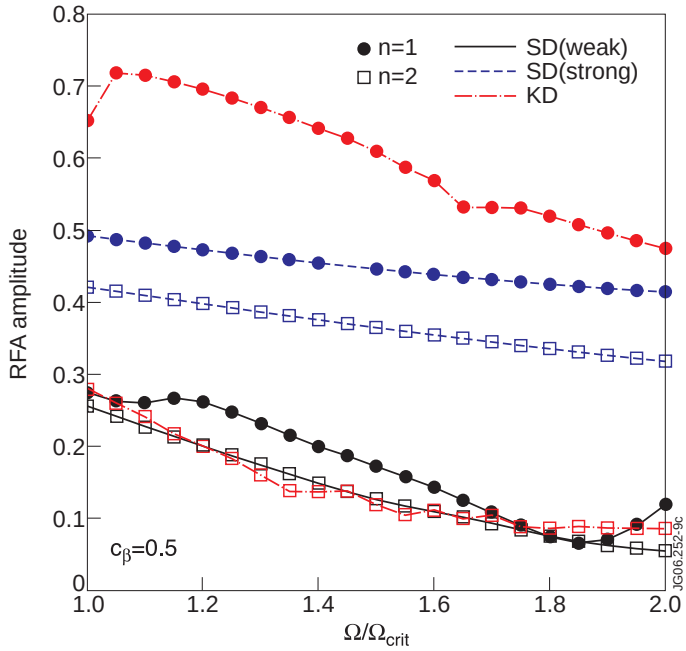

Fig 6 Comparison of RFA versus plasma rotation normalised to its critical value for n=1 and 2, at fixed C_β=0.5 for a JET-like equilibria. Results are presented for the kinetic damping (KD), and the strong ($\kappa_{||}$ =1.5) and weak ($\kappa_{||}$ =0.1) sound wave damping (SD) models implemented in MARS-F.

Magnetic braking experiments indicate a critical velocity for RWM destabilisation of $\tau_A\,\Omega$~0.5% near q~2, and also seem to be in reasonable agreement with calculations with MARS-F using the kinetic damping model. However it is likely the applied field plays a role in destabilising the mode and in the light of this, the data are interpreted as providing a threshold for error fields to drive locked mode above the no-wall β-limit. The data show an applied error field of $B_{2,1}/B_T$~2x10^{-4} in JET and DIII-D is sufficient to drive a locked mode, when $\beta_N>\beta_N$(no-wall), resulting in magnetic braking and likely RWM destabilisation. These results illustrate the importance of the proposed ITER error field correction system for high-β operation and give an initial indication that it should provide adequate correction.

The RFA experiments do indicate that the kinetic damping model implemented in MARS-F [2,9] is in reasonable agreement with experiment, but this in a regime of significant rotation between the plasma and mode where this theory would be expected to apply. At lower relative rotation, such as expected in ITER, other theories (e.g [15]) may be more applicable and further studies are required.

References

[1] Bondeson A., and Ward, D., Phys Rev Lett **72** (1994) 2709

[2] Bondeson A. and Chu M.S., Phys of Plas **3** (1996) 3013

[3] Fitzpatrick R., Phys of Plas **9** (2002) 3459

[4] Betti, R. and Friedberg J., Phys Rev Lett **74** (1995) 2949

[5] Gimblett C.G., and Hastie, R.J., Phys of Plasmas **7** (2000) 258

[6] Reimerdes H., *et al*., Phys. Plasmas **13** (2006) 056107.

[7] Reimerdes H., *et al*., Phys. Rev. Lett. **93**, 135002 (2004).

[8] Garofalo A M, *et al*, Phys. Plasmas 10 (2003) 4776

[9] Liu Y.Q., et al., Phys. Plasmas **7**, (2000) 3681

[10] Hender TC *et al* in *Fusion Energy* 2004 (Proc. 20th Int. Conf. *Vilamoura, Portugal, 2004*) (Vienna: IAEA) CD-ROM EX/P2-22 and http://www.naweb.iaea.org/napc/physics/fec/fec2004/index.html

[11] Fitzpatrick R and Hender T C., *Phys. Fluids* **B3** (1991) 644

[12] ITER Physics Basis, 1999 *Nucl. Fusion* **39** 2137.

[13] Garofalo A M et al, this conf Paper EX-7-1Ra

[14] Buttery R J. *et al Nucl. Fusion* **39** (1999) 1827

[15] Hu Bo and Betti R, *Phys Rev Lett* **93**, 105002(2004)

Acknowledgements

This work was partly supported by the UK Engineering and Physical Sciences Research Council, by the European Communities under the contract of Association between EURATOM and UKAEA, and by the US Department of Energy under DE-FG02-89ER54461, DE-FG03-95ER54309, DE-AC02-76CH03073 and DE-FC02-04ER54698. The views and opinions expressed herein do not necessarily reflect those of the European Commission. This work was partly conducted under the European Fusion Development Agreement.